Finally, it is interesting to note that, in fluid solvents, the earliest spectroscopic changes observed in Mb at room temperature occur within a few picoseconds of photodissociation (*13*). Because this time scale is comparable to the shear relaxation time of the aqueous solvent, the solvent response to the fastest conformational changes is expected to resemble that of an elastic solid. Picosecond-resolved optical studies of our system may therefore show that the fastest conformational changes of a protein appear similar in water and in a glass.

REFERENCES AND NOTES

1. H. Frauenfelder and P. G. Wolynes, *Science* **229**, 337 (1985); H. Frauenfelder, S. G. Sligar, P. G. Wolynes, *ibid.* **254**, 1598 (1991); H. Frauenfelder and P. Wolynes, *Phys. Today* **47**, 58 (1994).
2. R. H. Austin, K. W. Beeson, L. Eisenstein, H. Frauenfelder, I. C. Gunsalus, *Biochemistry* **14**, 5355 (1975).
3. E. R. Henry, J. H. Sommer, J. Hofrichter, W. A. Eaton, *J. Mol. Biol.* **166**, 443 (1983).
4. A. Ansari, C. M. Jones, E. R. Henry, J. Hofrichter, W. A. Eaton, *Science* **256**, 1796 (1992).
5. W. Doster, S. Cusack, W. Petry, *Nature* **337**, 754 (1989).
6. R. J. Loncharich and B. R. Brooks, *J. Mol. Biol.* **215**, 439 (1990); J. Smith, K. Kuczera, M. Karplus *Proc. Natl. Acad. Sci. U.S.A.* **87**, 1601 (1990).
7. D. Beece *et al.*, *Biochemistry* **19**, 5147 (1980).
8. N. Agmon and J. Hopfield, *J. Chem. Phys.* **79**, 2042 (1983); E. R. Henry, J. Hofrichter, J. H. Sommer, W. A. Eaton, in *Hemoglobins: Structure and Function*, A. Schnek and C. Paul, Eds. (Edition de l'Université de Bruxelles, Brussels, 1983), pp. 193–203; J. Hofrichter *et al.*, *Biochemistry* **24**, 2667 (1985).
9. P. J. Steinbach *et al.*, *Biochemistry* **30**, 3988 (1991).
10. J. Kuriyan, S. Wilz, M. Karplus, G. Petsko, *J. Mol. Biol.* **192**, 133 (1986).
11. D. G. Lambright, S. Balasubramanian, S. G. Boxer, *Chem. Phys.* **158**, 249 (1991).
12. W. D. Tian, J. T. Sage, V. Šrajer, P. M. Champion, *Phys. Rev. Lett.* **68**, 408 (1992).
13. M. Lim, T. A. Jackson, P. A. Anfinrud, *Proc. Natl. Acad. Sci. U.S.A.* **90**, 5801 (1993); T. A. Jackson, M. Lim, P. A. Anfinrud, *Chem. Phys.* **180**, 131 (1994).
14. A. Ansari, C. M. Jones, E. R. Henry, J. Hofrichter, W. A. Eaton, *Biochemistry* **33**, 5128 (1994).
15. H. A. Kramers, *Physica* **7**, 284 (1940); P. Hänggi, P. Talkner, M. Borkovec, *Rev. Modern Phys.* **62**, 251 (1990).
16. J. Jäckle, *Rep. Progr. Phys.* **49**, 171 (1986); C. A. Angell, *Science* **267**, 1924 (1995).
17. A model clarifying the relation between interconversion of conformational substates and the stretched exponential time course of conformational relaxation has been proposed by S. J. Hagen and W. A. Eaton (unpublished results). In this model the stretched relaxation reflects a redistribution of molecules from one distribution of conformational substates to another at lower energy, subject to the simple kinetic rule that all transition states are at approximately the same energy. The stretched exponential is a natural consequence of the interconversion of substates occurring on the same time scale as the change in the overall average structure of the molecule. Interconversion of conformational substates and conformational relaxation are parts of the same process.
18. J. L. Green and C. A. Angell, *J. Phys. Chem.* **93**, 2880 (1989).
19. C. Womersley, *Comp. Biochem. Physiol.* **70B**, 669 (1981); J. H. Crowe, L. M. Crowe, J. F. Carpenter, C. Aurell Wistrom, *Biochem. J.* **242**, 1 (1987).
20. Before analysis of the data, it was essential to correct the raw photolysis difference spectra for the intrinsic temperature dependence of both the Mb and MbCO spectra. This multistep correction is described elsewhere (*21*).
21. S. J. Hagen, J. Hofrichter, W. A. Eaton, unpublished results.
22. B. F. Campbell, M. R. Chance, J. M. Friedman, *Science* **238**, 373 (1987).
23. V. Šrajer and P. Champion, *Biochemistry* **30**, 7390 (1991).
24. N. Agmon, *ibid.* **27**, 3507 (1988); N. Agmon, *J. Phys. Chem.* **94**, 2959 (1990).
25. Because this model treats the protein and its environment as stiff and nonrelaxing on the time scale of ligand rebinding, the solvent does not exert dissipative influences that affect the diffusion constant of the moving ligand; we therefore do not include a solvent-viscosity dependence in these rates [N. Agmon and S. Rabinovich, *J. Chem. Phys.* **97**, 7270 (1992)].
26. Previous studies on Mb embedded in polyvinyl alcohol (PVA) discussed the question of the suppression of conformational substate interconversion in solid media (*2*) [A. Ansari *et al.*, *Biophys. Chem.* **26**, 337 (1987); I. Iben *et al.*, *Phys. Rev. Lett.* **62**, 1916 (1989)]. However, Mb in PVA shows complex and multiphasic kinetics above 200 K. These cannot be interpreted in the absence of spectral data on kinetic hole burning and conformational relaxation. Furthermore, the crossing of the ligand rebinding curves at different temperatures in PVA implies conformational relaxation as the explanation for the multiple nonexponential phases (*9*).
27. E. Mayer, *Biophys. J.* **67**, 862 (1994); W. Doster, T. Kleinert, F. Post, M. Settles, in *Protein-Solvent Interactions*, R. Gregory, Ed. (Dekker, New York, 1993), pp 375–385.
28. J. L. Green, J. Fan, C. A. Angell, *J. Phys. Chem.* **98**, 13780 (1994).
29. I. Schlichting, J. Berendzen, G. N. Phillips, R. M. Sweet, *Nature* **371**, 808 (1994); T.-Y. Teng, V. Šrajer, K. Moffat, *Nature Struct. Biol.* **1**, 701 (1994).
30. J. Hofrichter *et al.*, *Methods Enzymol.* **232**, 387 (1994).
31. E. R. Henry and J. Hofrichter, *ibid.* **210**, 129 (1992).

32. We thank A. Szabo, P. Wolynes, and R. Zwanzig for helpful discussions and C. Austen Angell for suggesting the use of trehalose as a glass.

29 March 1995; accepted 12 June 1995

Binding of CO to Myoglobin from a Heme Pocket Docking Site to Form Nearly Linear Fe–C–O

Manho Lim, Timothy A. Jackson, Philip A. Anfinrud*

The relative orientations of carbon monoxide (CO) bound to and photodissociated from myoglobin in solution have been determined with time-resolved infrared polarization spectroscopy. The bound CO is oriented ≤7 degrees from the heme normal, corresponding to nearly linear Fe–C–O. Upon dissociation from the Fe, CO becomes trapped in a docking site that orientationally constrains it to lie approximately in the plane of the heme. Because the bound and "docked" CO are oriented in nearly orthogonal directions, CO binding from the docking site is suppressed. These solution results help to establish how myoglobin discriminates against CO, a controversial issue dominated by the misconception that Fe–C–O is bent.

To understand how the structure of a protein affects its function, it is crucial to know the structures of intermediates in the reaction pathway. Myoglobin (Mb), a protein that reversibly binds small ligands such as O_2 and CO, has long served as a model system for probing protein control of ligand binding and discrimination (*1*). The active binding site in Mb consists of an iron(II)-containing porphyrin, known as a heme, embedded within the hydrophobic interior of the globular protein. It is well known that the protein environment modulates the activity and selectivity of the heme: CO binds to free heme about 10^3 to 10^4 times as strongly as O_2 (*2*) but binds to the heme in Mb only 30 times as strongly as O_2 (*3*). Because CO is produced endogenously by the metabolism of heme (*4*), discrimination against this toxic ligand is thought to be biologically important.

A structural basis for discrimination against CO was implicated by the crystal structures of liganded Mb and model heme compounds: it was found that CO binds to Mb in a bent Fe–C–O geometry (*5*) but binds to model hemes in a linear geometry (*6*). It was presumed that the protein forces CO to bind in a bent geometry, thereby reducing the affinity of the heme for CO (*2*, *7*). Because O_2 binds to Mb (*8*) and model hemes (*9*) in a similar bent configuration, the steric hindrance imposed by the protein on bound O_2 was presumed to be negligible. This mechanism for reducing the binding affinity of Mb for CO seems compelling. Indeed, it has become a classic example of the relation between structure and function in proteins (*10*). However, the premise that Fe–C–O is bent in MbCO (*11*, *12*) and the assumption that bending is functionally important (*13*) remain controversial.

The angle of CO relative to the heme plane normal of MbCO has been determined by a variety of techniques, some of which are detailed in Table 1. The x-ray and neutron diffraction crystal structures provide the strongest evidence for a bent Fe–C–O, with the CO orientation ranging from 19° to 60°. The discrepancies between $P2_1$ and $P6$ crystal structures might result from differences in crystal packing: $P6$ crystals contain more water and therefore might be a better model for MbCO in solution

Department of Chemistry, Harvard University, Cambridge, MA 02138, USA.

*To whom correspondence should be addressed.

(*14*). It has been suggested that the estimated uncertainty for the 1.5 Å x-ray and the 1.8 Å neutron diffraction structures might be as great as ±24° and ±27°, respectively (*11*). Consequently, these crystallographic methods determine the CO orientation rather coarsely. In contrast, polarized infrared (IR) measurements, which are capable of much higher precision, suggested that the CO is oriented <10° from the heme plane normal (*15*). Consistent with this result, recent analysis of heme-CO vibrational spectra disfavored any significant Fe–C–O bending in MbCO (*11*). A recent ab initio study of the heme prosthetic unit suggested that the CO orientation is largely determined by the proximal histidine: When the proximal histidine was constrained to x-ray coordinates, the CO orientation was 46° or 35°, depending on whether or not the distal histidine was included in the optimization; when the proximal histidine was allowed to relax, the CO orientation was along the heme normal (*16*). Molecular dynamics simulations of MbCO revealed a CO orientation of 3° (*17*), or between 2.1° to 6.5°, depending on the protonation state of the distal histidine (*18*). Clearly, the orientation of CO bound to Mb is controversial.

While an understanding of ligand discrimination requires accurate knowledge of the orientation of bound CO, it is crucial also to know the orientation of unbound CO in Mb*CO, the putative transient intermediate in the binding pathway. Two recent structures of Mb*CO, obtained by photolyzing MbCO crystals at cryogenic temperatures, provide some insight into this state (Table 1). Upon dissociation from the heme iron, CO becomes trapped in the heme pocket with the nearest atom less than 1.9 Å from the bound carbon position; whether the C or O is closer is not determined (*19, 20*). The unbound CO orientations reported for the $P2_1$ and *P*6 structures differ by 24°. Even if the structures were in complete agreement, it is not clear if the structures of Mb*CO at cryogenic temperatures are transferable to liquid solution at physiological temperatures. Because the effects of crystal packing and cryogenic temperatures are not yet fully understood, one should be careful when interpreting subtle details obtained from such crystal structures.

Table 1. Orientation of CO relative to heme plane normal (θ_{eq}) in MbCO and Mb*CO determined in crystals and in liquid solution.

Sample	Method	Resolution (Å)	θ_{eq} (degrees)	Reference
		MbCO		
$P2_1$ crystal (260 K)	X-ray	1.5	39 (78%)–60 (22%)†	(*5*)
$P2_1$ crystal (40 K)	X-ray	1.7	39	(*19*)
$P2_1$ crystal	Neutron	1.8	47 (58%)–44 (42%)†	(*42*)
*P*6 crystal‡(277 K)	X-ray	2.0	19	(*14*)
*P*6 crystal‡ (85 K)	X-ray	1.9	32	(*20*)
$P2_1$ and $P2_12_12_1$ crystals	Polarized IR	—	<10	(*15*)
Solution (283 K)	Photoselection	—	≤7	This work
		*Mb*CO*		
*P*6 crystal‡ (20 K)	X-ray	1.5	90 (±20)	(*20*)
$P2_1$ crystal (40 K)	X-ray	1.7	66	(*43*)
Solution (283 K)	Photoselection	—	67 to 90§	This work

†Two orientations of CO with differing occupancies were resolved. ‡Asp^{122}→Asn mutant of MbCO; this mutation, remote from the heme, facilitates the growth of *P*6 crystals. §The equilibrium orientation depends on the orientational probability distribution function for unbound CO. With an experimentally estimated distribution function, the orientation is calculated to be 90°; a delta function distribution yields 67°.

The need for accurate structural data determined under physiologically relevant conditions is evident. Photoselection spectroscopy (*21, 22*) is ideally suited for this problem. Using this technique, we have been able to study in liquid solution the orientation of CO in both MbCO and Mb*CO. We have observed a nearly linear Fe–C–O conformation for bound CO and have discovered a heme pocket docking site in which unbound CO is constrained to lie approximately parallel to the plane of the heme.

Determination of the CO orientation by photoselection spectroscopy is possible because spectroscopic transitions for both heme and CO are polarized along specific directions in the molecular frame (Fig. 1). When a solution of MbCO is illuminated with linearly polarized light, hemes oriented along the polarization direction absorb light preferentially. The ligands bound to these "photoselected" hemes are dissociated with high quantum efficiency, leading to a loss of bound CO and the production of metastable Mb*CO, that is, CO located near but not bound to the heme iron. If the CO is oriented at a particular angle θ relative to the heme plane normal, the ratio of its IR absorbance polarized perpendicular and parallel to the photolysis polarization, $\Delta A^{\perp}/\Delta A^{\parallel}$, is a simple analytic function of θ (*21*) (Fig. 2)

$$\frac{\Delta A^{\perp}}{\Delta A^{\parallel}} = \frac{4 - \sin^2\theta}{2 + 2\sin^2\theta} \quad (1)$$

In low-temperature glasses, where the protein orientation is frozen and ligand rebinding is slow, the polarized IR spectra can be measured with conventional IR spectrometers (*23*). In solution, where rotational tumbling of the protein randomizes the orientation of the photoselected hemes, the measurement must be made on a time scale that is short compared to the rotational diffusion

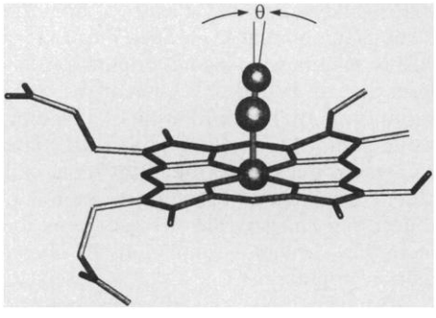

Fig. 1. The heme-CO coordinate system: θ is the angle between C–O and the heme plane normal. For a range of wavelengths, including our photolysis wavelength of 527 nm, the heme is well described as a circular absorber, that is, the spectroscopic transition is in the plane of the heme with equal contribution from the two orthogonal components (*41*). The vibrational transition of CO is assumed to be along the CO bond axis, an excellent assumption for dissociated CO as well as for bound CO when θ is small.

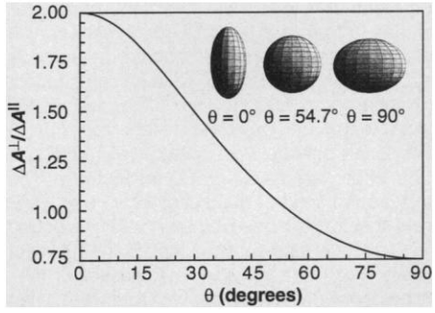

Fig. 2. The theoretical ratio of perpendicular and parallel polarized absorbance, $\Delta A^{\perp}/\Delta A^{\parallel}$, plotted versus the angle between C–O and the heme plane normal, θ. The ratio is 2 when C–O is oriented along the heme normal and 0.75 when orthogonal to the heme normal. Consequently, the ratio of perpendicular and parallel polarized absorbance is a sharp indicator of CO orientation. (**Inset**) The polarized IR absorption ellipsoids for CO when θ = 0°, 54.74°, and 90°, assuming randomly oriented circular heme absorbers are photolyzed with horizontally polarized light. For example, the major and minor dimensions of the θ = 0° ellipsoid are proportional to the absorption measured when the probe is polarized perpendicular and parallel to the photolyzing polarization, respectively. The absorption anisotropy disappears (the ellipsoid becomes spherical) when θ = 54.74°, the so-called "magic angle."

time, which is 8 ns for Mb in H_2O at 288 K (*24*). Consequently, this structural determination requires picosecond time resolution (*25*).

The time-resolved polarized absorbance spectra of photolyzed MbCO are shown in Fig. 3. The features are labeled A and B states, following Alben *et al.* (*26*). The negative-going A states retrace the equilibrium IR spectrum of MbCO and correspond to the photolysis-induced depletion of bound CO. The positive-going B states correspond to CO dissociated from the heme iron but trapped within the protein. The integrated absorbance of unbound CO is significantly less than that of bound CO, accounting for the poorer signal-to-noise ratio of the B state spectra.

The A state spectra reveal two prominent features, denoted A_1 and A_3, with A_1 blue-shifted relative to A_3. The ratio $\Delta A^{\perp}/\Delta A^{\parallel}$ is nearly constant (1.931 ± 0.02) across these features, demonstrating that the two A states are oriented at a similar angle. According to the theoretical curve of Fig. 2, the ratio 1.931 ± 0.02 corresponds to $\theta = 9.7° \mp 1.5°$. To generate that curve, the following assumptions were made: the orientational distribution of CO is a delta function in θ; the orientation of the heme in the laboratory frame is static on the 100-ps time scale; and the heme of MbCO is a perfectly flat circular absorber at the photolysis wavelength. Should any of these idealities not be realized, the equilibrium orientation of bound CO consistent with the measured ratio $\Delta A^{\perp}/\Delta A^{\parallel}$ must be revised to a smaller angle. For example, thermal motion of CO and its surroundings at 283 K ensure that the CO orientation is distributed about some equilibrium angle θ_{eq} and is therefore not a delta function in θ. From the estimated orientational distribution of bound CO (*27*), the equilibrium orientation consistent with the measured ratio $\Delta A^{\perp}/\Delta A^{\parallel}$ was calculated to be $\theta_{eq} = 7°$. Because we do not know the magnitude of heme libration on the 100-ps time scale nor the degree to which the heme deviates from a perfectly flat circular absorber (*28*), it is difficult to account quantitatively for their effects on the orientation measurement. Consequently, we cannot exclude the possibility that θ_{eq} is as small as 0°. We conclude therefore that CO bound to Mb is oriented $\leq 7°$ from the heme plane normal. Because the Fe–C–O bending motion at 283 K spans $\pm 4.5°$ (the estimated standard deviation of the orientational distribution function) (*27*), a range larger than our absolute uncertainty in the CO orientation, it is probably pointless to ascribe any functional significance to the small degree of Fe–C–O bending that may or may not occur in MbCO.

The B state spectra reveal two features, denoted B_1 and B_2, with B_1 blue-shifted relative to B_2. We suggested previously that these two features correspond to CO oriented oppositely within a heme pocket docking site (*29*). Recently, using 100-fs photolysis pulses, we found that the B state spectrum appears in ~0.5 ps, demonstrating that the docking site must be located within a few angstroms of the heme iron. Moreover, we also found that the B state spectrum persists for hundreds of nanoseconds, a time quite long compared with that required for CO to become trapped, thereby justifying use of the term "docking" site.

According to Fig. 3, the polarized absorbance ratio $\Delta A^{\perp}/\Delta A^{\parallel}$ for "docked" CO is much closer to 0.75 than it is to 2, demonstrating that CO rotates substantially upon dissociation from the heme iron. Unlike the polarized absorbance ratio measured for the A states, the ratio for the B states is vibration-frequency dependent, yielding information about both the equilibrium orientation of "docked" CO and the trajectories for CO motion within the docking site.

If the orientation of "docked" CO was a delta function in θ, that angle could be determined directly from the polarized absorbance ratio measured in the vicinity of the peaks of the two B states. According to Fig. 3, the two B states reveal a similar ratio, $\Delta A^{\perp}/\Delta A^{\parallel} = 0.856 \pm 0.03$, which corresponds to $\theta = 67° \mp 3°$. Of course, at physiological temperatures, the orientation of "docked" CO is not static but undergoes significant angular motion. Indeed, it undergoes end-to-end rotation on a picosecond time scale at 283 K (*29*). Consequently, the orientation of CO must be described by an orientational probability distribution function. Where this distribution function peaks, corresponding to the equilibrium orientation of "docked" CO (θ_{eq}), depends on the width and shape of the distribution function. For example, using the orientational distribution function estimated from integrated B state absorbance measurements (*29*), we recover $\theta_{eq} = 90°$ for both B states, in agreement with the suggestion that they are oriented oppositely (*30*). Therefore, we conclude that "docked" CO lies approximately in the plane of the heme.

The vibration-frequency dependence of the polarized absorbance ratio provides insight into the trajectories for CO motion within the docking site. Because the docking site is anisotropic, the center frequency of CO shifts from one B state to the other as it undergoes end-to-end rotation. Consequently, one might expect the frequency of CO at the transition state for end-to-end rotation to be centered between the peaks of the two B states. At the midpoint, the ratio $\Delta A^{\perp}/\Delta A^{\parallel}$ exhibits a maximum of ~1, demonstrating that the trajectory for end-to-end rotation passes through a transition state that has a component out of the plane of the heme. If this trajectory were to lie on a plane, that plane would be inclined from the heme plane by ~35° and the transition state would be oriented at least 55° from the heme plane normal (*31*). Such a trajectory would maintain a ligand orientation far from that for bound CO, even at the transition state, thereby inhibiting CO binding while permitting end-to-end rotation. The constraints imposed by the B state polarized absorbance ratio on ligand orientation and trajectories can provide stringent tests for molecular dynamics simulations of ligand motion in proteins.

Although the crystal structures of MbCO yield CO orientations quite different from that in solution, x-ray structures of Mb*CO at cryogenic temperatures (*19*, *20*) appear to be consistent with our solution results: (i) The vibrational spectra of "docked" CO produced by photolysis of MbCO at 5.5 K (*26*) and 283 K (*29*) are nearly the same, suggesting that the CO in Mb*CO becomes trapped in the same site at both cryogenic and ambient tempera-

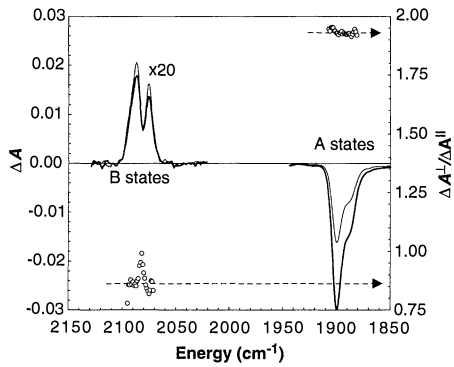

Fig. 3. Polarized IR absorption spectra and their ratio measured 100 ps after photolysis of $Mb^{13}CO$ in D_2O. The left axis corresponds to the photolysis-induced absorbance changes $\Delta A^{\perp}$ (thick lines) and $\Delta A^{\parallel}$ (thin lines); the right axis corresponds to their ratio $\Delta A^{\perp}/\Delta A^{\parallel}$ (open circles). The ratio is plotted where the absorbance exceeds ~25% of its maximum and has been corrected for fractional photolysis (*33*). The dashed lines correspond to the average A and B state ratios. The A and B state spectra were collected at 10.8% and 20% photolysis of $Mb^{13}CO$, respectively. The background and hot band contributions to the B state spectra have been removed (*29*). The bound ^{13}CO spectra represent the result of $>10^6$ laser pulses, each one providing a measure of the sample absorbance at a particular wavelength and polarization. The sample cell was rotated to a new position between laser pulses. Because the unbound ^{13}CO signal is much weaker, $>10^7$ laser pulses were required to attain the level of sensitivity shown. We used D_2O and ^{13}CO to shift the vibrational frequency of unbound CO into a region of greater solvent transparency, thereby enhancing the sensitivity of the measurements, which were made at 283 K.

tures; (ii) according to the two crystal structures, the nearest atom of unbound CO is ≤1.9 Å from the bound carbon position, consistent with the subpicosecond appearance of the B state spectrum in solution; and (iii) the equilibrium orientations of CO reported for the two crystal structures of Mb*CO differ by 24° but are, within experimental uncertainty, the same as that estimated for "docked" CO in solution.

The orientations for bound and "docked" CO found in this study differ from those of earlier polarized IR measurements. The notion of a bent Fe–C–O geometry was supported by low-temperature (*23*) as well as ambient-temperature (*21*) measurements, with the different A states reported to be bent at different angles ranging from 15° to 35°. The orientation of "docked" CO was unsettled, with one report arguing for isotropically oriented CO (*23*) and another for a temperature-dependent orientation (~31° at 300 K and ~80° at 150 K) (*32*). Although the underlying theory for determining angles with the photoselection technique is rigorous, there are a number of experimental pitfalls. For example, earlier determinations either neglected fractional photolysis effects or corrected for them incompletely (*33*), they did not account for the orientational distribution of CO, and they may have been compromised by systematic errors (*34*). Furthermore, if the photolyzing beam was not measurably larger than the probe beam, spatial nonuniformity of photolysis would have compromised the angle measurement further. In general, such experimental or analytical error would have the effect of reducing the difference between the equilibrium angles of bound and "docked" CO. Because the difference reported here is the largest measured, we conclude that the bound and "docked" CO orientations determined in this work are the most definitive to date.

From this work emerges the following picture. Carbon monoxide binds to Mb to form nearly linear Fe–C–O. Upon dissociation from the heme iron, CO becomes trapped in a docking site located within a few angstroms from the heme iron. The docking site constrains CO to lie approximately parallel to the plane of the heme, an orientation approximately orthogonal to that of bound CO. The orientational and spatial constraints imposed on CO by the docking site have the effect of slowing dramatically the rate of CO rebinding. Indeed, we have found recently that CO rebinds to Mb more than three orders of magnitude more slowly than to microperoxidase (*35*) or protoporphyrin, model systems that have no such docking site. The Mb docking site therefore facilitates efficient expulsion of this toxic ligand from the protein: we find that <2% of CO rebinds geminately at 32°C.

Presumably, the heme pocket docking site traps O_2 as well. If the orientational distribution of O_2 within the docking site is similar to that of CO, it would have significant overlap with the orientation of bound O_2: according to a 1.6 Å crystal structure of MbO_2 (*8*), O_2 is oriented 60° from the heme plane normal and points toward the site where CO becomes trapped. Consequently, the docking site would not be expected to inhibit O_2 binding nearly to the extent that it inhibits CO binding. Indeed, the rate of O_2 binding from the heme pocket docking site (*36*) is more than two orders of magnitude faster than what we measure for CO (*37*). Because the orientation of CO obtained from the crystal structure of MbCO differs from that in solution, might the structure of MbO_2 differ as well? Our solution measurements are in agreement with the crystal structures of model heme-CO compounds. Because model heme-O_2 compounds reveal a range of orientations (*9*) that agree, within experimental uncertainty, with that for MbO_2 (*8*), it seems likely that the orientation of O_2 remains significantly bent in solution.

Evidently, it is the overlap between the bound and docked ligand orientations that plays a significant role in modulating the relative rates of binding CO and O_2 from the heme pocket. To that end, the highly conserved residues circumscribing the heme pocket of Mb fashion a docking site that orientationally constrains the dissociated ligand and thereby influences the rates and pathways for ligand binding and escape.

REFERENCES AND NOTES

1. See B. A. Springer, S. G. Sliger, J. S. Olson, G. N. Phillips Jr., *Chem. Rev.* **94**, 699 (1994) and references therein.
2. J. P. Collman, J. I. Brauman, T. R. Halbert, K. S. Suslick, *Proc. Natl. Acad. Sci. U.S.A.* **73**, 3333 (1976).
3. E. Antonini and M. Brunori, *Hemoglobin and Myoglobin in Their Reactions With Ligands* (North-Holland, London, 1971).
4. S. A. Landaw, E. W. Callahan Jr., R. Schmid, *J. Clin. Invest.* **49**, 914 (1970).
5. J. Kuriyan, S. Wilz, M. Karplus, G. A. Petsko, *J. Mol. Biol.* **192**, 133 (1986).
6. S. M. Peng and J. A. Ibers, *J. Am. Chem. Soc.* **98**, 8032 (1976).
7. W. S. Caughey, *Ann. N.Y. Acad. Sci.* **174**, 148 (1970).
8. S. E. V. Phillips, *J. Mol. Biol.* **142**, 531 (1980).
9. J. P. Collman, R. R. Gagne, C. A. Reed, W. T. Robinsin, G. A. Rodley, *Proc. Natl. Acad. Sci. U.S.A.* **71**, 1326 (1974); G. B. Jameson *et al.*, *Inorg. Chem.* **17**, 850 (1978); G. B. Jameson *et al.*, *J. Am. Chem. Soc.* **102**, 3224 (1980).
10. L. Stryer, *Biochemistry* (Freeman, San Francisco, 1988).
11. G. B. Ray, X.-Y. Li, J. A. Ibers, J. L. Sessler, T. G. Spiro, *J. Am. Chem. Soc.* **116**, 162 (1994).
12. S. Hu, K. M. Vogel, T. G. Spiro, *ibid.*, p. 11187.
13. T. G. Traylor, *Acc. Chem. Res.* **14**, 102 (1981).
14. M. L. Quillin, R. M. Arduini, J. S. Olson, G. N. Phillips Jr., *J. Mol. Biol.* **234**, 140 (1993).
15. D. Ivanov *et al.*, *J. Am. Chem. Soc.* **116**, 4139 (1994).
16. P. Jewsbury, S. Yamamoto, T. Minato, M. Saito, T. Kitagawa, *ibid.*, p. 11586.
17. E. R. Henry, *Biophys. J.* **64**, 869 (1993).
18. P. Jewsbury and T. Kitagawa, *ibid.* **67**, 2236 (1994).
19. T.-Y. Teng, V. Šrajer, K. Moffat, *Nat. Struct. Biol.* **1**, 701 (1994).
20. I. Schlichting, J. Berendzen, G. N. Phillips Jr., R. M. Sweet, *Nature* **371**, 808 (1994).
21. J. N. Moore, P. A. Hansen, R. M. Hochstrasser, *Proc. Natl. Acad. Sci. U.S.A.* **85**, 5062 (1988).
22. A. Ansari and A. Szabo, *Biophys. J.* **64**, 838 (1993).
23. P. Ormos *et al.*, *Proc. Natl. Acad. Sci. U.S.A.* **85**, 8492 (1988).
24. J. Albani and B. Alpert, *Chem. Phys. Lett.* **131**, 147 (1986).
25. The time-resolved IR spectrometer used to determine the orientation of CO has been described elsewhere (*38*). The sample, ≈13 mM sperm whale $Mb^{13}CO$ in D_2O buffered with 0.1 M potassium phosphate, pD 7.5, was loaded into an IR cell with a 100-μm path and CaF_2 windows. The absorbance of the sample at the photolysis wavelength of 527 nm was 1.4. The MbCO was photolyzed with a linearly polarized laser pulse (35 ps, 527 nm) whose polarization direction was controlled electronically by a liquid-crystal polarization rotator. The photolyzed sample was probed 100 ps after photolysis with a linearly polarized IR probe pulse (200 fs, ~5 μm) whose transmitted intensity was spectrally resolved with an IR monochromator (3-cm^{-1} bandpass) and detected with a liquid-nitrogen–cooled InSb photodetector. The photodetector signal was normalized with respect to the probe intensity to obtain the transmittance of the sample at the wavelength selected by the monochromator. The photolysis-induced change of the sample absorbance, ΔA, was computed from sample transmittances measured with and without the photolysis pulse. During a wavelength scan, the photolysis polarization was alternated between parallel and perpendicular orientations, thereby recording both polarized spectra essentially simultaneously. The 1.2- to 1.5-kHz repetition frequency of the laser system permitted extensive signal averaging and led to the high-quality time-resolved spectra reported here.
26. J. O. Alben *et al.*, *Proc. Natl. Acad. Sci. U.S.A.* **79**, 3744 (1982).
27. We know of no direct measure of the orientational distribution of CO bound to the heme of Mb. We have used the frequency of the tilting Fe–C–O mode in $Fe(CO)_5$ (*40*) to estimate the potential energy function and hence the orientational distribution for axial-bound CO. Although the potential of mean force for the Fe–C–O bending motion in MbCO can differ from that for axial-bound CO in gas-phase $Fe(CO)_5$, this estimate should be approximately correct.
28. If the heme were ruffled (nonplanar), there would be a nonzero transition moment along the direction of the heme normal at the photolysis wavelength. Consequently, the "photoselection" would be less selective, reducing the polarization anisotropy of the photolyzed sample. If the heme were an elliptical absorber, the polarization anisotropy for large θ would depend on the azimuthal orientation φ. For small θ, the difference between a circular and elliptical absorber is negligible.
29. M. Lim, T. A. Jackson, P. A. Anfinrud, *J. Chem. Phys.* **102**, 4355 (1995).
30. The orientational distribution was assumed to be cylindrically symmetric, which is likely not the case for the anisotropic environment that surrounds the "docked" CO. That is, the potential energy surface describing the motion of CO may be different in θ than along the azimuthal angle φ. Consequently, the equilibrium orientation could deviate somewhat from 90°, and the two B states might in fact be oriented at slightly different angles. Nonetheless, the equilibrium orientation for each B state is much closer to 90° than it is to 67°. The uncertainty of the equilibrium orientation of CO is small compared with the width of the orientational distribution, which spans ±27° at 283 K (the estimated standard deviation of the orientational distribution function) (*29*).
31. Although other trajectories for end-to-end rotation

are not excluded by our data, the orientational constraints imposed on the ligand by the docking site suppresses trajectories with small θ at the transition state.
32. L. J. Rothberg, M. Roberson, T. M. Jedju, *Proc. SPIE* **1599**, 309 (1991).
33. Corrections to the measured ratio $\Delta A^{\perp}/\Delta A^{\parallel}$ due to fractional photolysis of an optically thin sample have been proposed previously (*22*, *39*). We go one step further and calculate the correction for fractional photolysis in an optically thick sample, which, under our experimental conditions, is nearly twice that predicted for an optically thin sample. The validity of this correction has been verified experimentally.
34. B. Locke, T. Lian, R. M. Hochstrasser, *Chem. Phys.* **190**, 155 (1995).
35. Microperoxidase is a water-soluble heme-peptide (pH 7) formed by enzymatic digestion of cytochrome c oxidase. One face of the heme is exposed to solvent while the other is in contact with and covalently bound to the peptide through a histidine linkage. The electronic spectra of microperoxidase-CO and MbCO are similar, suggesting that the electronic environment of microperoxidase models that of Mb.
36. K. A. Jongeward *et al.*, *J. Am. Chem. Soc.* **110**, 380 (1988).
37. Oxygen rebinds biexponentially with its slow phase approximately 2 orders of magnitude faster than what we measure for CO rebinding.
38. P. A. Anfinrud, M. Lim, T. A. Jackson, *Proc. SPIE* **2138**, 107 (1994).
39. P. A. Hansen, J. N. Moore, R. M. Hochstrasser, *Chem. Phys.* **131**, 49 (1989).
40. C. W. F. T. Pistorius and P. C. Haarhoff, *J. Chem. Phys.* **31**, 1439 (1959).
41. A. K. Churg and M. W. Makinen, *ibid.* **68**, 1913 (1978); W. A. Eaton and J. Hofrichter, *Methods Enzymol.* **76**, 175 (1981).
42. X. Cheng and B. P. Schoenborn, *J. Mol. Biol.* **220**, 381 (1991).
43. K. Moffat, personal communication.
44. This work is supported in part by NIH grant DK45306, the National Science Foundation Young Investigators Program, the Beckman Foundation, and the Mitsubishi Kasei Corporation. We thank J. S. Olson for generously supplying the Mb.

13 February 1995; accepted 19 May 1995

Boron Nitride Nanotubes

Nasreen G. Chopra, R. J. Luyken, K. Cherrey, Vincent H. Crespi, Marvin L. Cohen, Steven G. Louie, A. Zettl*

The successful synthesis of pure boron nitride (BN) nanotubes is reported here. Multiwalled tubes with inner diameters on the order of 1 to 3 nanometers and with lengths up to 200 nanometers were produced in a carbon-free plasma discharge between a BN-packed tungsten rod and a cooled copper electrode. Electron energy-loss spectroscopy on individual tubes yielded B:N ratios of approximately 1, which is consistent with theoretical predictions of stable BN tube structures.

The discovery of carbon nanotubes in 1991 (*1*) has generated intense experimental and theoretical interest in such structures. Theoretical studies of carbon tubes suggest that their electrical properties will range from metallic to semiconducting, depending on the tube diameter and chirality (*2*, *3*). This leads to a diverse spectrum of properties, but it is also highly complex from an applications point of view, as the tube chirality and diameter are impossible to control with the use of present synthesis methods. Most carbon nanotubes observed are composed of multiple coaxial tubes, with the spacing between tube walls being approximately the graphite interplanar distance. The properties of a multiwalled carbon nanotube are expected to be even more complex, because they will depend sensitively on the detailed geometry of each constituent tube.

Authors of a recent tight-binding calculation have proposed that nanotubes might also be formed from hexagonal boron nitride (BN) (*4*). Local density approximation and quasi-particle calculations indicate that BN tubes are semiconducting with a gap of roughly 5.5 eV [versus 5.8 eV (*5*) for bulk hexagonal BN] and that the gap is nearly independent of tube diameter, chirality, and the number of tube walls (*6*). The calculated uniform electronic properties of BN tubes contrast sharply with the heterogeneity of carbon tubes [and other carbon-containing tubes such as those formed from BC_2N (*7*) and BC_3 (*8*)] and suggest that BN tubes may have significant advantages for applications. Although previous studies have demonstrated the existence of BN filaments with diameters on the order of 100 nm (*9*), as well as carbon-containing nanotubes with the stoichiometry of BC_2N (*10*, *11*) and BC_3 (*10*), pure BN nanotubes have not been reported. We describe here the synthesis and stoichiometric characterization of multiwalled BN nanotubes.

Boron nitride nanotubes were synthesized in a plasma arc discharge apparatus similar to that used for carbon fullerene production (*12*). To avoid the possibility of carbon contamination, no graphite components were used in the synthesis. The insulating nature of bulk BN prevents the use of a pure BN electrode. Instead, a pressed rod of hexagonal BN 3.17 mm in diameter was inserted into a hollow tungsten electrode with an outer diameter of 6.3 mm, forming a compound anode. The cathode consisted of a rapidly cooled pure copper electrode. During discharge, the environmental helium gas was maintained at 650 torr and the dc current was ramped from 50 to 140 A to maintain a constant potential drop of 30 V between the electrodes. A dark gray soot deposited on the copper cathode, in contrast to the case of carbon tube growth, in which typically a more cohesive cylindrical deposit with a hard crustlike shell forms on the cathode. After the arcing was complete, pieces of solidified tungsten were found spattered inside the chamber, indicating that the temperature at the anode during synthesis exceeded 3700 K, the melting point of tungsten.

Characterization of the cathodic deposit was accomplished with transmission electron microscopy (TEM) with the use of a JEOL JEM 200CX electron micro-

Fig. 1. TEM image of a BN soot sample on an amorphous support grid. Dark arrows point out one long BN multiwalled nanotube. The light arrow identifies another nanotube.

Department of Physics, University of California, Berkeley, and Materials Sciences Division, Lawrence Berkeley Laboratory, Berkeley, CA 94720, USA.

*To whom correspondence should be addressed.